Aligned Nanofibrous Net Deposited Perpendicularly on Microridges Supports Endothelium Formation and Promotes the Structural Maturation of hiPSC-Derived Cardiomyocytes

Feng Tian, Linlin Yin, Peiran Lin, Yurong Liu, Wenlong Wang, Yong Chen, Yadong Tang

Aligned nanofibrous net deposited perpendicularly on microridges supports endothelium formation and promotes the structural maturation of hiPSC-derived cardiomyocytes

Feng Tian [a], Linlin Yin [a], Peiran Lin [a], Yurong Liu [a], Wenlong Wang [b], Yong Chen [b], and Yadong Tang [a*]

[a] *School of Biomedical and Pharmaceutical Sciences, Guangdong University of Technology, Guangzhou, 510006, China*

[b] *School of Mechanical and Electrical Engineering, Guangzhou University, Guangzhou, 510006, Chinac[b] PASTEUR, Département de Chimie, Ecole Normale Supérieure, PSL University, Sorbonne Université, CNRS, Paris 75005, France*

*E-mail: tangyadong@gdut.edu.cn

Abstract

Cell alignment widely exists in various *in vivo* tissues and plays also a crucial role in the construction of *in vitro* models, such as vascular endothelial and myocardial models. Recently, microscale and nanoscale hierarchical topographical structures are drawing increasing attention for engineering *in vitro* cell alignment. In the present study, we fabricated a micro/nano hierarchical substrate based on soft lithography and electrospinning to assess the synergetic effect of both aligned nanofibrous topographical guidance and off-ground culture environment provided by the substrate on the endothelium formation and the maturation of human induced pluripotent stem cell-derived cardiomyocytes (hiPSC-CMs). The morphology, proliferation and barrier formation of human umbilical vein endothelial cells (HUVECs) as well as the alignment, cardiac specific proteins and maturity related genes expression of hiPSC-CMs on the aligned-nanofiber /microridges (AN-MR) substrate were studied. Compared with glass slide and the single aligned nanofiber substrate, AN-MR substrate enhanced the proliferation, alignment, and cell-cell interaction of HUVECs and improved the length of sarcomere and maturation-related gene expression of hiPSC-CMs. To evaluate the functional maturation of hiPSC-CMs, the response of the hiPSC-CMs on different substrates to two typical cardiac drugs (isoproterenol and E-4031) were tested and analyzed, showing that the hiPSC-CMs on AN-MR substrates were more resistant to drugs than those in the other groups which was related to the higher maturity of the cells. Overall, the proposed micro/nano hierarchical substrate supports the *in vitro* endothelium formation and enhances the maturation of hiPSC-CMs, which shows great potential to be applied in the construction of *in vitro* models and tissue engineering.

Keywords: alignment, endothelial cell, hiPSC-CMs, mature, drug evaluation

1. Introduction

Cell alignment widely exists in *in vivo* tissues and organs [1], such as vascular endothelial cells (ECs), skeletal muscle cells, neuron cells and cardiomyocytes (CMs). The alignment of cells also plays a critical role in various cell behaviors, tissue maturation and regeneration. For example, the proper alignment of cardiomyocytes provides an optimal coupling of electrical signal propagation, synchronized cell contraction, and calcium cycling, which is significant for efficient cardiac function [2, 3]. Additionally, aligned endothelial cells, which are highly oriented along the direction of blood vessels, are known to act as guidance cues for Schwann cell migration and nerve regeneration [4]. Therefore, *in vitro* engineering of cell alignment is indispensable for tissue engineering applications and in vitro drug screening model construction.

Various approaches have been explored to achieve *in vitro* cell alignment, e.g. mechanical stretch, fluid shear stress, and topographical patterning [1]. Thereinto, topographical patterning is the mostly studied and applied approach to engineer cell alignment. Various anisotropic scaffolds or patterned substrates have been developed to mimic the native micro/nanostructures of the cellular microenvironment based on micro- or nano- fabrication techniques, including electrospinning [5], soft lithography [6], freeze-drying [7] and 3D printing [8]. It has also been demonstrated that many types of cells are mechanosensitive and their behaviors vary in response to micro- and nanoscale topographic cues [9]. For instance, Li et al. [10] developed a series of electrospun PCL fibers with varied diameter and orientation to culture endothelial cells and found micro- and nano- topographies have different effects on cell alignment and behaviors. Park et al. [11] fabricated a size-tunable nerve guidance conduit with hundreds of microchannels for enhanced nerve regeneration by the alignment of cells.

The vascular endothelium is composed of a monolayer of endothelial cells that lines the inner surface of blood vessels [12]. And the shape, alignment and maturation of ECs play a crucial role on vascular tone, thrombosis, and vascular wall inflammation [13]. In particular, the alignment of endothelial cells may regulate biological signals such as intracellular protein expression, cytoskeletal organization, intercellular connectivity and endothelial barrier function [13]. Therefore, many researchers have attempted to simulate the alignment of ECs for *in vitro* endothelium modeling or blood vessel tissue engineering. Kim et al. [14] developed a cell culture well insert with a collagen gel-coated and aligned nanofiber membrane (Col-ANM) for the

construction of an effective endothelial barrier model. Morimotol et al. [15] proposed a microfluidic system with a culture insert containing a collagen vitrigel membrane for applying shear flow to align endothelial cells align along the flow direction and mimic the structure of unidirectionally aligned endothelium tissue.

Among various *in vivo* aligned cells, cardiomyocytes are relatively unique due to the constant spontaneous contraction and relaxation. Human induced pluripotent stem cell derived cardiomyocytes (hiPSC-CMs) hold great potential for myocardial tissue engineering and the construction of *in vitro* cardiac model because of the abundant availability and the recapitulation of human cardiac physiological and functional features [16]. Despite progress, the generated hiPSC-CMs compared with adult cardiomyocytes remain an immature state in terms of morphology, metabolism, and functionality, exhibiting similarities to the CMs in fetal heart [17, 18]. Furthermore, lethal arrhythmias can occur when immature CMs applied for myocardial regeneration [17]. Thus, further effort should be performed to enhance the maturation of hiPSC-CMs. Up to now, many literatures have focused on accelerating the hiPSC-CMs maturation by utilizing a series of biophysical cues such as patterned topographical features [19], mechanical and electrical stimulation [20]. Thereinto, patterned topographical cues were widely applied to effectively promote the maturation of hiPSC-CMs. For example, Kumar et al. [21] fabricated an aligned polycaprolactone (PCL)-gelatin coaxial nanofiber patch using electrospinning, which improved the alignment, the expression of cardiac specific proteins and the drug response of hiPSC-CMs. E. Huethorst et al. [22] enhanced the maturation of hiPSC-CMs using a dual microgradient substrate (8 ~ 100 μm in space, 5 nm ~1 μm in depth) and showed only the deepest and widest region (8~30 μm wide and 0.85~1 μm deep) had a significantly higher percentage of hiPSC-CMs with an increased eccentricity, elongation and orientation.

Although nanoscale and microscale structures have been demonstrated to promote cell alignment and the maturation of hiPSC-CMs to some extent, sole nano-structure does not possess the microscale features found in native tissue, which results in a lack of microscale cellular organization necessary for *in vivo* mechanical function [23]. In addition, the larger microscale patterns generally result in a lack of unidirectional guidance between cells [24]. Micro/nano hierarchical structures have been demonstrated to exhibit further advantages over the single micro- or nano- structures. Yeo et al. [25] prepared a hierarchical alginate/PCL scaffold

comprising both microscale and nanoscale topographical structures by the combination of electrospinning and 3D printing, which exhibited that the cell orientation and myotube formation of C2C12 cells cultured in the 3D hierarchical structure were significantly better than those in the single micro- or nano- groups. Yang et al. [26] developed a substrate with well-defined hierarchical triple-scale sequentially aligned topographies, giving rise to the enhanced cell alignment and osteogenic differentiation compared to the other single and double scale substrates.

Previously, we prepared a culture patch composed of gelatin monolayer nanofibrous net supported with a honeycomb microframe. The support of the microscale frame and the monolayer nanofibrous net structure with high through-hole percentage can provide cells with an off-ground culture environment. Different from the conventional culture environment, cells cultured under off-ground are with both upper and lower contact with medium, rather than the only upper medium contact, which largely improves cell-medium exchange. We have successively demonstrated that the off-ground culture environment facilitated the differentiation of hiPSCs into cardiomyocytes [27] and motor neurons [28], and allowed more effective culture of primary neurons than conventional methods [29]. Recently, we reported that HUVECs on the culture patch exhibited improved proliferation, cell-cell interaction and barrier formation compared with the conventional nanofiber membrane and track-etched polycarbonate (PC) membrane due to the fewer binding sites offered for cells and also the enhanced metabolism under off-ground culture [30]. All of the above findings demonstrated the advantages of the off-ground culture for cell behaviors especially resulted by the improved cell-medium exchange and metabolism. Therefore, we speculate that the combination of aligned topographical guidance with this kind of off-ground culture environment may achieve synergistic effect on endothelium formation and hiPSC-CMs maturation.

Herein, we developed an aligned-nanofiber /microridges (AN-MR) substrate based on soft lithography and electrospinning and studied its effect on endothelium formation and the maturation of hiPSC-CMs. Firstly, we evaluated the effect of AN-MR substrates on the phenotype, proliferation and cell-cell interaction of HUVECs. Then, we extensively compared the maturity of hiPSC-CMs on AN-MR substrates by studying the phenotype of cells, the expression of specific proteins and cardiac maturation related genes. The drug sensitivity of the

hiPSC-CMs on different substrates were also analyzed to further explore the effect of AN-MR substrate on hiPSC-CMs maturation.

2. Materials and methods

2.1 Fabrication of AN-MR substrate

AN-MR substrate was prepared using soft lithography combined with electrospinning, which was schematically shown in Figure 1(a). Firstly, the microgroove was fabricated by soft lithography. Briefly, a silicon wafer was spin-coated with a 40 μm thick positive photoresist layer (AZ40XT, Futurrex, USA) at 500 rpm for 10 s and 1500 rpm for 20 s. After being prebaked at 65 °C for 1 min, 95 °C for 2 min and 120 °C for 8 min, the photoresist was exposed to UV light through a photo-mask and was then post-baked 30 s at 65°C and 2 min at 105 °C. Then the photoresist was developed in AZ319MIF developer for 1 min. After rinsing with DI water, the mask with patterned resist was dried with a nitrogen gun and treated with trimethylchlorosilane (TMCS, Sigma) for 1 min to prevent adhesion. Then, a mixture of PDMS base and curing agent (10:1, w/w, Sylgard 184, Dow Corning, USA) was poured onto the master mold and cured at 80 °C for 3 h. After peeling off from the master, a PDMS substrate with 40 μm spacing, 20 μm width and 40 μm height of microgrooves could be obtained.

Next, the micropatterned PDMS substrate was applied for collecting nanofibers. For electrospinning, gelatin (10 wt%) was dissolved in a solvent mixture of DI water, ethyl acetate and acetic acid with a volume ratio of 10:14:21. Then the gelatin solution was loaded in a 1 mL syringe and ejected by a syringe pump (LSP02-1B, Baoding Lange Constant current Pump Co., LTD, China) at a flow rate of 0.3 mL/h. A high voltage of 13-15 kV was applied between spinneret and collector with a distance of 15-18 cm. In this work, aligned nanofibers were generated via parallel electrode method [31] by using two ground-connected metal bars with a gap of 2-3 cm. The micropatterned PDMS substrate was placed between the two parallel metal bars for collecting gelatin nanofibers. Then the obtained substrates with nanofibers were dried overnight under vacuum to remove residual solvent. Afterwards, the electrospun gelatin nanofibers were crosslinked in an ethanol solution containing 0.2 M 1-ethyl-3-(dimethylaminopropyl) carbodiimide hydrochloride (EDC) and 0.2 M N-hydroxyl succinimide (NHS) for 3 h. Finally, the substrate was rinsed with ethanol for three times and dried in a

vacuum for 24 h for the next cell culture studies. During experiment, glass slide and glass slide covered with aligned gelatin nanofibers (AN) were applied as control groups for comparison.

2.2 Scanning electron microscopy

The surface topography of the prepared AN-MR substrate was characterized using scanning electron microscopy (SEM, TM3030, Hitachi, Japan) at 15 kV. The orientation of the gelatin nanofibers was measured by analyzing the SEM images using ImageJ.

2.3 Cell culture

2.3.1 HUVEC culture

Human umbilical vein endothelial cells (HUVECs, ScienCell) were maintained in endothelial cell medium (ScienCell) with 10% fetal bovine serum, 1% endothelial cell growth supplement and 1% penicillin/streptomycin at 37 °C in 5% CO_2. For cell seeding, substrates were placed in 12-well plates and overnight under UV light, and then immersed in Dulbecco's phosphate-buffered saline (DPBS, Genview) for 2-6 h. Then, HUVECs with 90% confluence were washed with DPBS, removed with a 0.25% trypsin/ethylenediaminetetraacetic acid (trypsin-EDTA, Gibco) solution and seeded onto the experimental substrates at a concentration of 2×10^4 cells/cm^2.

2.3.2 Differentiation and culture of hiPSC-CMs

Human induced pluripotent stem cells (hiPSC-U1, CELLAPY) were cultured in a Matrigel (hESC-Qualified Matrix, 1:100 diluted, equivalent to ~0.008 mg Matrigel protein per square centimeter, Corning, America) coated 12-well plate, which were maintained with PSCeasy® II complete medium (CELLAPY, China) at 37°C with 5% CO_2. The medium was refreshed daily. HiPSC-CMs were obtained through two steps by differentiation and glucose starvation-based purification. Thereinto, hiPSCs were differentiated into CMs as previously described with the protocol of Lian et. al [32]. Briefly, after hiPSCs reached about 75% confluence (day 0), the medium was changed to RPMI 1640 medium containing 2% B27 minus insulin supplement (both from Gibco) and 10 μM CHIR 99021 (Selleckchem). On day 1, the medium was switched to RPMI 1640 / B27 minus insulin supplement. On day 3, the cells were exposed to RPMI 1640

/B27 supplement without insulin containing 5 μM IWP 2 (Tocris). On day 5, the medium was replaced with RPMI 1640 plus B27 minus insulin supplement. On day 7, the RPMI media was supplemented with B27+ insulin and was then refreshed every other day (48 h). Generally, spontaneous contraction could be observed on day 9-10. To further purify cardiomyocytes and eliminate non-cardiomyocytes, the differentiated cells were subjected to glucose starvation [33] using medium composed of RMPI 1640 without D-glucose containing 2% B27 supplement and 1% Penicillin/Streptomycin (Gibco) for three days and then the medium was switched to RPMI 1640/B27 supplement for 24 h. After two rounds of the purification, the hiPSC-CMs were ready to be seeded and cultured on the three substrates (glass, AN, AN-MR). Prior to cell seeding, the substrates were coated with Matrigel and incubated overnight at 37 °C. Purified cardiomyocytes were dissociated using 0.25% trypsin-EDTA (Gibco) for 5-7 min and seeded on the substrates with a density of 2×10^4 cells/cm^2. During culture, medium (RPMI 1640/B27 + Insulin) was changed every other day.

2.4 Live/dead assay

The viability of HUVECs and hiPSC-CMs was determined by using a Live/Dead assay kit (Abbkine) according to the manufacturer's protocol after 24 h of culture. Thereinto, green fluorescent LiveDye was used to mark living cells, while red fluorescent NucleDye was to view dead cells. Briefly, the culture medium was removed firstly, followed by gently washing with PBS, and then the samples were incubated in the live/dead solution composed of PBS, LiveDye (2%, (v/v)) and NucleDye (1.5%, (v/v)) at 37°C for 15 min. Finally, the stained samples were observed under an inverted fluorescence microscope (IX71, Olympus, Japan). Cell viability was calculated by analyzing the fluorescence images via ImageJ software.

2.5 CCK-8 assay

CCK-8 assay was performed to assess the proliferative ability of HUVECs at 24 h, 48 h and 72 h of culture on glass, AN and AN-MR substrates. In brief, 10 μL CCK-8 reagent dissolved in 100 μL culture medium was added to each well and incubated for 4 h at 37°C. Afterwards, the solution was transferred to a 96-well plate and the optical density (OD) at 450 nm was measured using a microplate reader (Infinite F50, TECAN, America).

2.6 Immunofluorescence

Cells were fixed in 4% (v/v) paraformaldehyde solution (PFA, Biosharp, China) for 15 min, permeabilized with 0.1% (v/v) Triton X-100 (Sigma-Aldrich) for 30 min, and then blocked with a blocking solution (0.1% Tween 20 / 5% normal goat serum / 5% normal donkey serum / 3% bovine serum albumin / PBS) for 1 h at room temperature. After washing with PBS, the samples were incubated with primary antibodies, *i.e.*, anti-alpha actinin (1:150, Abcam), anti-cTnT (1:100, Abcam), anti-VE Cadherin (1:200, Abcam) and anti-Paxillin (1:150, Abcam) overnight at 4°C. Following primary antibody incubation, samples were washed three times with PBS at room temperature, followed by 4 h of incubation with the corresponding secondary antibodies, *i.e.*, donkey anti-rabbit IgG H&L (Alexa Fluor 488) (1:250, ab150073, Abcam), goat anti-mouse IgG H&L (Alexa Fluor 594) (1:500, ab150116, Abcam). Additionally, to evaluate the orientation of cells, the cytoskeleton of HUVECs and hiPSC-CMs were stained with Alexa fluor-488 phalloidine (1:250, Abcam) for 20 min. Then, the cell nuclei were stained with 4', 6-diamidino-2-phenylindole (DAPI, 1 mg/ml, Beijing Solarbio Science & Technology Co., Ltd.) for 15 min. Finally, samples were visualized with an inverted fluorescent microscope (IX71, Olympus, Japan) and/or a confocal microscope (LSM800, Carl Zeiss, Germany). The analysis of cell orientation and cell area were performed with ImageJ software. The aspect ratio of cells was defined as long axes/short axes. The circularity index of cells was defined as 4π area/perimeter^2 as previous described [34].

2.7 Real-time quantitative polymerase chain reaction (RT-qPCR)

Total RNA of hiPSC-CMs was isolated using FastPure® Cell/Tissue Total RNA Isolation Kit (Vazyme Biotech Co., Ltd, America) and their respective complementary DNA (cDNA) was then synthesized utilizing the SweScript RT I First Strand cDNA Synthesis kit (Servicebio Biotech Co., Ltd, China) as per manufacturer's instructions. Gene expression of MYH6, MYH7, MLC2a, MLC2v and cTnI were quantified from 1 μL of template cDNA using ChamQ Universal SYBR qPCR Master Mix (Vazyme Biotech Co., Ltd, America) with specific primers (Integrated DNA Technologies) and detected by LightCycler® 96 Real-time PCR system (Roche). All assays were performed in triplicate and the relative expression levels of each single

gene were normalized using GAPDH and calculated using the $2^{-\Delta\Delta Ct}$ method.

2.8 Drug testing

Drug experiments on hiPSC-CMs were preformed after 6 days of culture on glass, AN and AN-MR substrates. Isoproterenol (0.2 and 0.5 μM, MedChemExpress) and E-4031 (50 and 100 nM, MedChemExpress) were added to the RPMI 1640/B27 medium, respectively. After incubation with the medium containing drug for 20 min at 37 °C, the beating video of hiPSC-CMs was captured with a CCD camera (Guangzhou YUESUI Biotechnology Co., Ltd.) with 1024×968 resolution and a frame rate of 60 fps. And the data were analyzed by using a custom-coded motion tracking MATLAB program as previously described [35, 36]. Briefly, the frame images output via beating videos were divided into an array of macroblocks containing 16 by 16 pixels, and the motion of each macroblock was determined by an exhaustive search block matching algorithm. Meanwhile, the motion velocity tracking was obtained with two subsequent characteristic peaks (contraction and relaxation) by averaging the vector amplitudes over a specific region.

2.9 Statistical analysis

The data was presented as the means ± standard deviation (SD). Two independent groups were compared using the Student's t-test, while multiple group variance was compared using one-way analysis of variance (ANOVA), followed by Tukey's test. The levels of significant were considered as *P < 0.05, **P<0.01.

3. Results and Discussion

3.1 Morphology of AN-MR substrate

In this study, we designed a micro/nano hierarchical substrate with microgrooves placed on the bottom and aligned nanofibers perpendicularly attached on the top of the microridges. The PDMS having ridges/grooves micropatterns microridges with an overall size of 1 cm × 1 cm were designed to provide mechanical support for the nanofibers, while the aligned gelatin nanofibers were used to guide the arrangement and adhesion of cells so as to mimic the extracellular microenvironment [37]. Considering the size of cells, the stability of the whole

structure and the deposition of the nanofibers to form an off-ground culture condition, the dimension of the microridges was finally designed to be 20 μm in width, 40 μm in height and 40 μm in spacing, which also referenced the dimensions in the other reports [38, 39].

As shown in Figure 1(a), the microridges and aligned nanofibers were fabricated by soft lithography and electrospinning, respectively. The SEM morphologies of the fabricated PDMS microridges and AN substrate were shown in Fig. S1(a) and (b), respectively. Fig. 1(b) shows a photograph of the fabricated AN-MR substrate, where the alignment of nanofibers could be observed faintly. The morphology of the substrate was then examined with SEM which was shown in Fig. 1(c), demonstrating the designed micro/nano hierarchical substrate was successfully achieved. During fabrication, by modulating the electrospinning time (<10 min), a monolayer of aligned nanofibers possessing high permeability supported with microridges could be achieved. The diameter and orientation distribution of the gelatin nanofibers were then measured using the ImageJ software as shown in Fig. 1(c-e). After crosslinking, the diameter of the nanofibers was increased from 359 ± 80 nm to 560 ± 90 nm, which might be due to the swelling of the fibers during the crosslinking process. And the angles between the nanofibers and the axial direction ranged from −20° to 20° and mainly concentrated in the range of ±10°. The pore size of the aligned nanofibrous net was then measured with image J software, as shown in Figure.1(f). There was no hole larger than 18 μm^2 observed on AN-MR substrate and most of holes were smaller than 8 μm^2, which was sufficient to provide enough support for cell growth and adhesion on the substrate. Therefore, the obtained aligned nanofibrous net supported with PDMS microridges could provide an off-ground culture condition for cells. Previously we have reported that the off-ground environment for cells could increase the exposure area of cells to medium thus facilitate the diffusion of nutrients and cellular uptake[27]. Next, the effect of the off-ground structure with aligned nanofibers on endothelium formation and the maturation of hiPSCs-derived cardiomyocytes would be further studied.

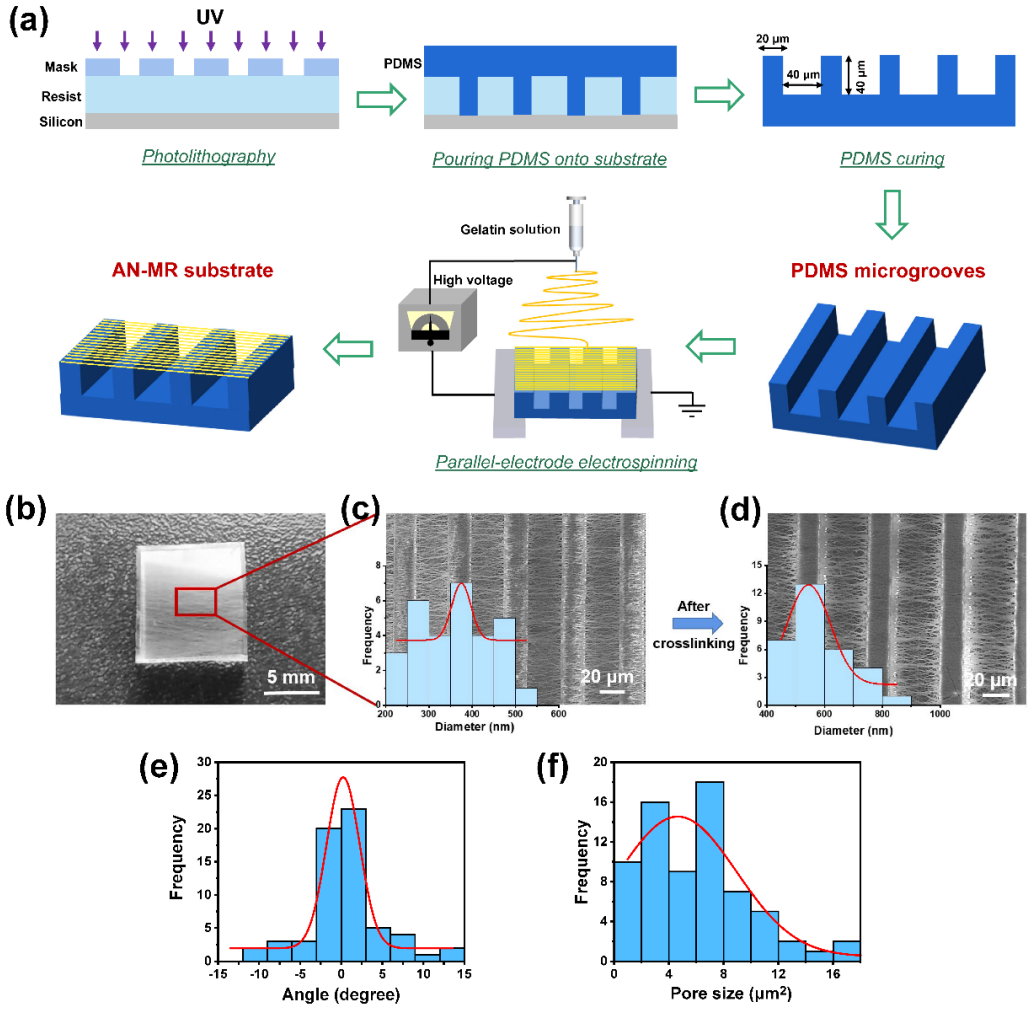

Figure 1. Schematic illustration and characterization of AN-MR substrate. (a) Fabrication process of AN-MR substrate. (b) Photograph of AN-MR substrate. (c-d) SEM images of AN-MR substrate and diameter distribution of gelatin nanofibers before (c) and after (d) crosslinking. (e-f) Fiber orientation distribution (e) and pore size distribution (f) of the gelatin nanofibrous net on AN-MR substrate.

3.2 HUVECs culture and endothelium formation on AN-MR substrate

Highly aligned cellular structures have been discovered in many native tissues, such as blood vessels, skeletal muscle, and cardiac tissues [40, 41]. HUVECs have been intensively adopted to construct *in vitro* vascular models [42]. To verify the hypothesis that the prepared micro/nano hierarchical substrates can effectively guide cellular alignment and endothelium formation, HUVECs were cultured on different substrates (glass, AN, AN-MR). Live/dead fluorescence images (Fig. 2(a)) showed that the vast majority of cells (green color) remained viable and only few cells (red color) were dead on the three types of substrates after 24 h of culture. The cell

viability on glass, AN and AN-MR substrates all exceeded 90% by calculating the ratio of live cells and dead cells (Fig. 2(b)), indicating that the AN-MR substrates fabricated in this study had good biocompatibility and were suitable for cell growth. The proliferation of HUVECs cultured on glass, AN and AN-MR substrates for 24 h, 48 h and 72 h were then evaluated by CCK-8 assay. The assessment of cell numbers in samples based on optical density (OD) recordings (Fig. 2(c)) indicated that the growth of HUVECs was similar on the three kinds of substrates in the first 24 h. However, after 48 h and 72 h of culture, there was a significant increase in cell proliferation on AN and AN-MR substrates, which could be explained by that nanofibers mimic the porous topography of natural extracellular matrix (ECM) to enhance cell growth [43]. And the cellular growth on AN-MR substrate was relatively faster compared with that on AN substrate. In particular, the cell density reached around 8×10^4 cells/cm^2 when cultured on AN-MR substrate for 72 h, which demonstrated that the culture environment provided by the fabricated micro/nano hierarchical substrate effectively promoted the proliferation of HUVECs. In addition, it may be attributed to the high porosity and the off-ground state of the nanofiber layer, which promoted the nutrient supply and material exchange for cells. When cells were seeded on flat substrate, only the upper surface of cells can be exposed to the medium for substance exchange and metabolism. However, the off-ground state of the nanofibrous net in AN-MR substrate could provide cells with both upper and lower surface contact with the medium, thus increasing cell-medium exchange and metabolism. Therefore, cells under off-ground culture exhibited improved proliferation, which is also consistent with our previous findings [27, 30].

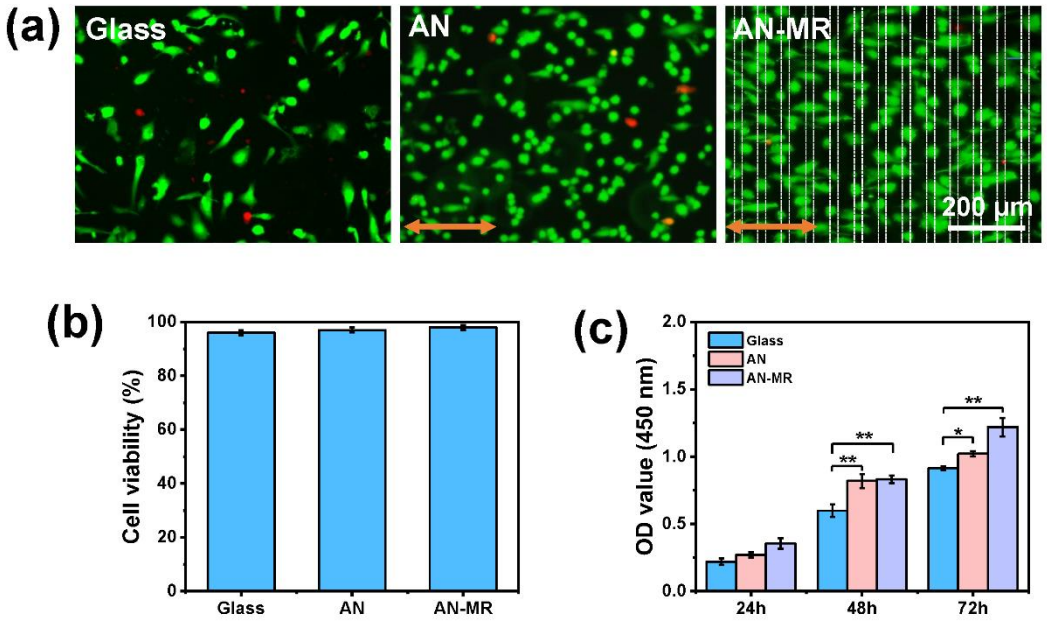

Figure 2. Viability and proliferation of HUVECs on glass slide, AN and AN-MR substrates. (a) Fluorescence (live = green; dead = red) images of HUVECs after cultured on the three substrates for 24 h. The microridges were marked with white dotted line and the direction of nanofibers were marked with orange double arrow. (b) Cell viability of HUVECs on three substrates from (a). (c) Proliferation of HUVECs on different substrates at 24 h, 48 h and 72 h, quantified by CCK-8 assay. *P < 0.05 and **P < 0.01.

Besides, we also studied preliminarily the preference of cells grown on different types of areas in AN-MR group. Due to the spreading length of the aligned cells was larger than the ridge width, most of cells grew across both ridge and off-ground locations as can be seen from the fluorescent images. Therefore, we analyzed the number of cell nuclei located atop ridges and in off-ground area, respectively. For the nuclear across both areas, the area with larger nulear area was determined to be the preferable area during counting. As shown in Fig. S3, we found that there was 71.6±6.6% of nuclei located on off-ground area while 24.8±4.9% atop ridges. Considering that the off-ground area was twice of the area atop ridges but the percentage of nuclei was more than twice the percentage atop ridges, it seems like cell nuclei tended more to stay on the off-ground culture area. It might also be attributed to the larger surface exposure area of cells to medium under off-ground culture.

Furthermore, cell morphology and cell orientation were visualized via cytoskeleton staining and analyzed by imageJ. As shown in Fig. 3(a), the cytoskeleton stained with phalloidin (red) showed an extended morphology along the direction of nanofibers, demonstrating that the

morphology and alignment of HUVECs were significant affected by the surface topography differences. To quantitatively represent the alignment of HUVECs, the nuclei aspect ratio and orientation of HUVECs after 2 days of culture were measured. The nuclei aspect ratio was calculated by dividing the length of the major axis by that of the minor axis. The nuclei aspect ratio was measured to be 1.33 ± 0.31 on glass, while the ratios on AN and AN-MR substrates were greater than 2 (Fig. 3(b)), which further demonstrated the alignment effect of nanofibers on cell orientation. There was no significant difference between AN group and AN-MR group. Simultaneously, cell alignment was further evaluated by measuring the angle between the fiber alignment direction and the axis of HUVECs. HUVECs cultured on glass were dispersed over the whole area with arbitrary angles, while more than 90% of the cells were aligned with orientation angles within ±10° in AN and AN-MR groups (Fig. 3(c)). The statistical results confirmed that the fabricated AN-MR substrate could effectively induce cell alignment which was similar to the conventional aligned nanofibers.

VE-cadherin, as an endothelial-specific adhesion protein, plays a crucial role in regulating the formation of adherens junctions and maintaining the endothelial barrier integrity [44]. As shown in Fig. 3(d), the cells on all of the three substrates exhibited strong positive staining with VE-cadherin at cell-to-cell contact regions, and the formation of VE-cadherin in AN and AN-MR groups was more continuous than in glass group. Then, we further measured the intercellular junction width for evaluating the integrity of the formed endothelial barrier by using image J software according to the references [45, 46]. The junctions formed on AN and AN-MR substrates were tighter compared with that in glass group (15.14 ± 3.44 μm), and the junction width was smallest in AN-MR group (10.18 ± 2.08 μm), as shown in Fig. 3(e). It has been demonstrated that the narrower width of tight junctions correlated with the stronger cell-cell interaction and enhanced barrier integrity [46, 47]. The result represented that tighter cell-cell junction and improved barrier integrity were formed on AN-MR substrates. Previously, Julie C et al. [48] found that endothelial cells were more likely to bind tightly on a compliant substrate. In this work, aligned nanofibers were attached on glass for AN substrate, while suspended on the relatively soft PDMS microridges for AN-MR substrate. Thus, the aligned nanofibrous net provided a more compliant culture environment for cellular growth to form tighter cell junctions. Recently, we reported a gelatin nanofibrous net and found that HUVECs showed

enhanced cell-cell interaction and stronger barrier integrity on the nanofibrous net compared than the conventional substrates [30]. The result of intercellular junction on AN-MR substrate was similar to that on the reported nanofibrous net, which was due to the similar cell culture condition provided by AN-MR substrate and nanofibrous net.

From the above results, it can be inferred that the micro/nano hierarchical substrate displayed sufficient cytocompatibility to promote the adhesion, alignment and proliferation of HUVECs and enhanced the integrity of the formed endothelial barrier. This advantage could be attributed to the synergistic effect of the aligned topographic cues and the constructed off-ground cell culture environment provided by AN-MR substrate.

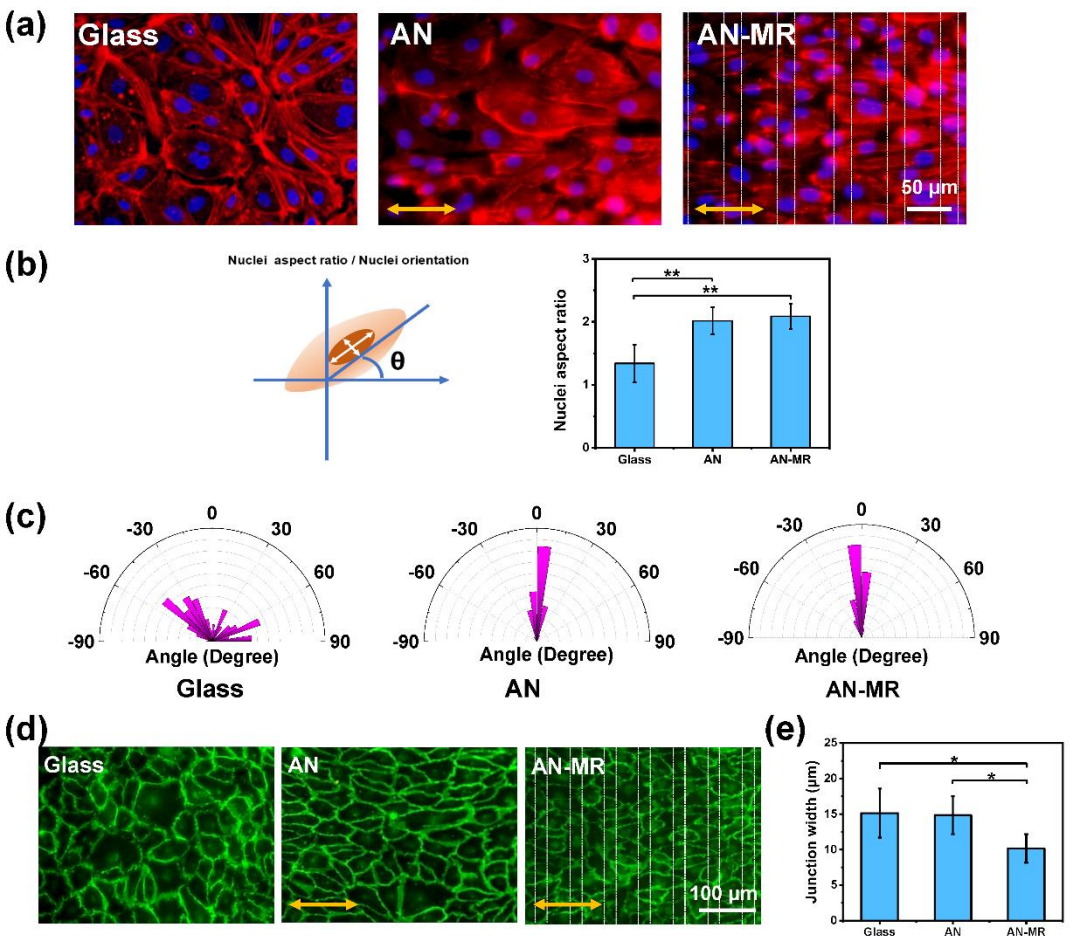

Figure 3. Morphology and cell-cell interaction of HUVECs on glass, AN and AN-MR substrates. (a) Immunofluorescence staining images of HUVECs cultured on glass, AN and AN-MR substrates for 72 h. Cells were stained with DAPI (blue, nuclei) and F-actin (red, cytoskeleton). (b) Nuclei aspect ratio of HUVECs on the three substrates. (c) Nuclei orientations distribution of HUVECs on the three substrates from (a), n = 50. (d) Immunofluorescence images of

HUVECs cultured on the three substrates, stained with VE-cadherin for characterizing the integrity of endothelial layer (green) and DAPI for nuclei (blue). (e) Junction width were quantified and compared from (d), n = 30. The microridges were marked with white dotted line and the direction of nanofibers were marked with orange double arrow.*P < 0.05 and **P < 0.01.

3.3 Structural maturation of hiPSC-CMs promoted by AN-MR substrate

Although the utility of hiPSC-CMs for cardiotoxicity evaluation and regenerative medicine was validated, it still faces hurdles due to the immature and fetal-like phenotypes of the cells [49]. The adult CMs in native cardiac tissue were cylindrical in shape with anisotropic myofilaments, and aligned for obtaining optimal contractility capacity, implying that cell alignment plays a key role in the maturation of hiPSC-CMs [22, 50]. Thus, considering the effective guidance effect of the fabricated AN-MR substrate on cell alignment, its effect on the growth, alignment and maturation of hiPSC-CMs was further studied.

As shown in Fig. 4(a), hiPSCs were differentiated according to the previous method and the differentiated hiPSC-CMs were purified by glucose starvation [16]. Then the purified hiPSC-CMs were seeded on glass, AN and AN-MR substrates, respectively. Firstly, the viability of the reseeded hiPSC-CMs was evaluated by live/dead assay. It was shown that the hiPSC-CMs on all of the three different substrates showed high cellular viability (> 90%) (Fig. 4(b) and Fig. S2), which further verified the good cytocompatibility of AN-MR substrate. The morphology of hiPSC-CMs on the three kinds of substrates was then studied by cytoskeleton fluorescence staining. As shown in Fig. 4(c), the orientation of the hiPSC-CMs on AN and AN-MR substrates was mostly along the direction of nanofibers, whereas the cells on glass did not exhibit any detectable preferential direction, which was similar to the results of HUVECs. It demonstrated that the aligned nanofiber could successfully guide the alignment of hiPSC-CMs no matter on plain substrate or on microridges.

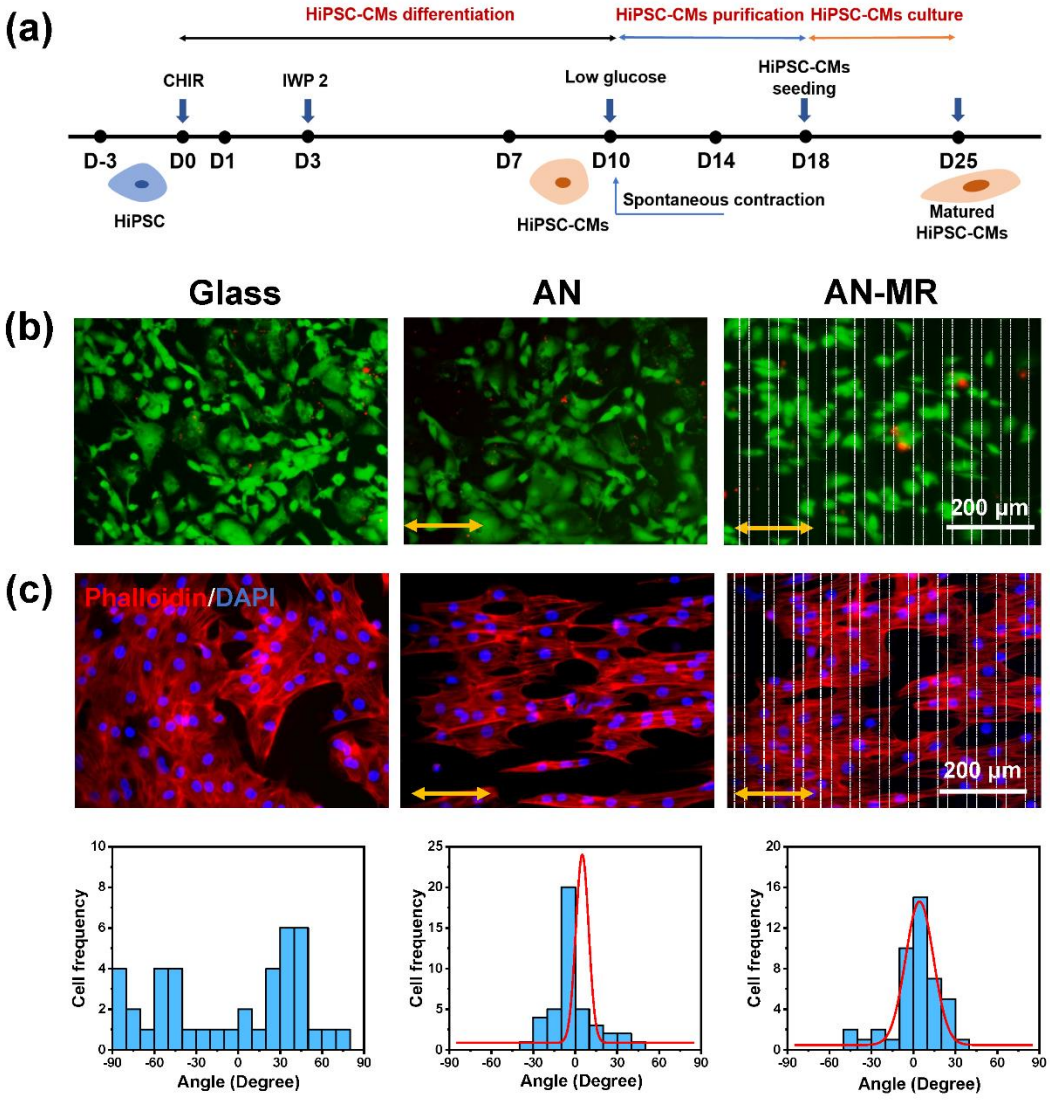

Figure 4. (a) Flowchart of hiPSC-CMs differentiation, purification and reseeding in this study. (b) Viability analysis of hiPSC-CMs cultured on glass, AN and AN-MR substrates for 24 h by fluorescence microscopy, stained with LiveDye (live, green) and NucleDye (dead, red). (c) Fluorescent staining of F-actin (red, phalloidin) and orientation distribution of the hiPSC-CMs grown on the three substrates for 3 days showing distinct morphologies and alignment (n = 50). The microridges were marked with white dotted line and the direction of nanofibers were marked with orange double arrow.

In addition, cTnT, which is a typical CM-specific protein, was positively expressed in the hiPSC-CMs cultured on the three kinds of substrates (Fig. 5(a)). The ordered arrangement of cTnT morphology along the direction of nanofibers was found on AN and AN-MR substrates, while glass did not induce a defined orientation and cells displayed a random distribution of troponin T across the cytoplasm. Specially, the expression of cTnT showed a much clearer

sarcomeric organization on AN-MR substrate than the other two groups, which was reported as a characteristic of mature CMs [27]. These results demonstrated that the aligned nanofibers of AN and AN-MR substrates could reassemble the myofibrils of hiPSC-CMs to be parallel to the long axis of hiPSC-CMs.

Sarcomere is the fundamental contractile unit of CMs [51] and the length of sarcomere which is the distance between two Z-discs is recognized to be an indicator of CM maturation [52]. The hiPSC-CMs on different substrates were immunostained with sarcomere specific protein α-actinin. As shown in Fig. 5(b), the hiPSC-CMs on all of three substrates showed a positive expression of α-actinin. In detail, the myofibril was more elongated and the spatial organization of myofibrils was more highly ordered and clearer in AN-MR group, compared with that in the other groups. Meanwhile, we noticed that many hiPSC-CMs cultured on AN substrate showed typical rod-shape morphology of mature/adult CMs compared to the other groups. The cells on AN-MR substrate did not show the expected more rod-shape morphology, which might be explained by the different and complex 3D culture environment provided by AN-MR substrate. To further study the effect of different substrates on the maturation of hiPSC-CMs, the length of sarcomeres was measured by using image J software as shown Fig. 5(c). The result revealed that the hiPSC-CMs cultured on glass, AN and AN-MR substrates showed the mean sarcomere lengths of 1.39 ± 0.29, 1.58 ± 0.23, 1.96 ± 0.31 μm, respectively. It has been reported that the sarcomere length of adult cardiomyocytes is within the range of 1.8-2.2 μm, while immature hiPSC-CMs exhibit a sarcomere length of approximately 1.5 μm [53]. The sarcomere lengths of hiPSC-CMs on AN-MR substrates were in accordance with the length of mature CMs, which indicated that the AN-MR substrate could promote the maturation of hiPSC-CMs at the level of sarcomere. Furthermore, cell length/width ratio and circularity are also recognized to be valuable analytical tools to determine the structural development and maturation of *in vitro* hiPSC-CMs [54, 55]. It has been reported that the phenotype of human adult CMs exhibit a length-to-width ratio of around 5~7 [56, 57]. To be able to compare the cell shape on different substrates with adult CMs values, we calculated the length/width ratio i.e. the major axis of the cell, divided by the minor axis. Fig. 5(d) showed that the length/width ratio of the hiPSC-CMs on AN-MR substrate was with an average value of 6.22, which was significantly higher than that on glass and AN substrate ($P < 0.01$). Additionally, the circularity index was measured

according to the previously reported method [34]. As shown in Fig. 5(e), the circularity index values of the hiPSC-CMs on AN and AN-MR substrates were significantly lower compared to the control, indicating that aligned nanofibers were capable of promoting cellular anisotropy. The circularity index in AN-MR group was further lower than that in AN group. Taken together, we posited that the AN-MR substrate could promote the structural organization of internal cytoskeleton of hiPSC-CMs, especially myofibril organization and sarcomere length development.

To further study the maturation status of hiPSC-CMs, qRT-PCR was performed to test the expression of 5 cardiac maturation related genes (MYH6, MYH7, MLC2v, MLC2a, and cTnI) in hiPSC-CMs after 6 days cultured on of the three kinds of substrates. As shown in Fig. 5(f), AN and AN-MR substrates greatly enhanced the expression levels of the 5 maturation related genes. Since the myosin heavy chain (MHC) isozymic transition from MHC-α (encoded by MYH6) to MHC-β (encoded by MYH7) was known as a key cardiac development/maturation marker [58], the ratio of MYH7 and MYH6 was calculated and shown in Fig. 5(g). A significant increase of MYH7/MYH6 ratio was found for AN-MR group compared with the other two groups. In addition, myosin light chain (MLC) protein isoforms also can change during maturation, so MLC2v/MLC2a ratio has been used as another key indicator of CMs maturation [59]. As shown in Fig. 5(h), the ratio of MLC2v and MLC2a on AN-MR substrate was significantly increased compared with the controls. The combination of two quantitative analyses confirmed the higher cell maturity on the proposed AN-MR substrate.

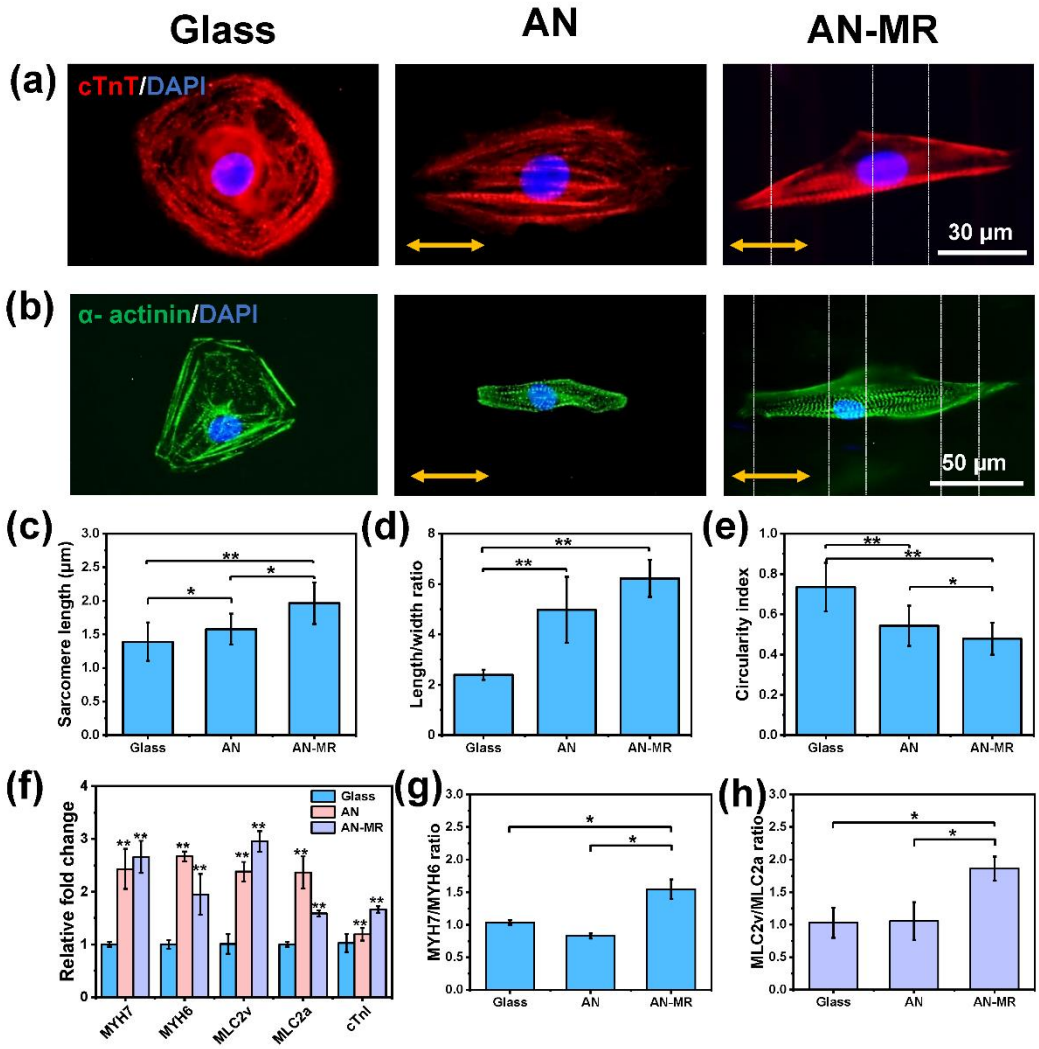

Figure 5. Phenotypic and structural maturation of hiPSC-CMs. (a-b) Immunofluorescence images of hiPSC-CMs cultured on glass, AN and AN-MR substrates for 6 days. The cells were stained for sarcomeric structural proteins (cTnT, red and α-actinin, green) and DAPI (blue). The microridges were marked with white dotted line and the direction of nanofibers were marked with orange double arrow. (c-e) Mean sarcomere length (c) length-to-width ratio (d) and circularity index (e) of the hiPSC-CMs cultured on different substrates measured using imageJ software, n = 10. (f) qRT-PCR analysis to examine the expression of relative maturation-related genes (MYH7, MYH6, MLC2v, MLC2a, cTnI) on the three substrates. Genes were normalized to GAPDH. (g) MYH7/MYH6 gene expression ratio. (h) MLC2v/MLC2a gene expression ratio. *$p < 0.05$; **$p < 0.01$.

3.4 Drug response of the hiPSC-CMs on AN-MR substrate

The maturation state of hiPSC-CMs has been demonstrated to determine the drug responsiveness [60, 61]. To further study the functional maturity, the hiPSC-CMs cultured on the three kinds of substrates were applied for drug tests using two typical drugs (ISP and E-4031)

with known clinical cardiac responses. The beating rate and beating velocity were analyzed using the real-time videos by a custom-coded motion tracking Matlab program. ISP is a β-adrenergic receptor agonist, which has been demonstrated to increase heart rate [62]. In the absence of ISP, there was no significant difference in the spontaneous beating rate of the hiPSC-CMs cultured on different substrates. With the application of 0.2 μM and 0.5 μM ISP, the beating rate and contraction velocity of hiPSC-CMs both increased on all of the three substrates (Fig. 6(a)and 6(b)). We further analyzed the beating rate change after drug action (Fig. 6(c)), showing the increase by 68.2% and 86.3% on glass, 47.71% and 70.77% on AN substrate, 54.73% and 70.33% on AN-MR substrate at the concentration of 0.2 μM and 0.5 μM ISP, respectively. Especially, the beating rate change at 0.5 μM ISP in glass group was significantly larger than that in AN and AN-MR groups ($P < 0.05$).

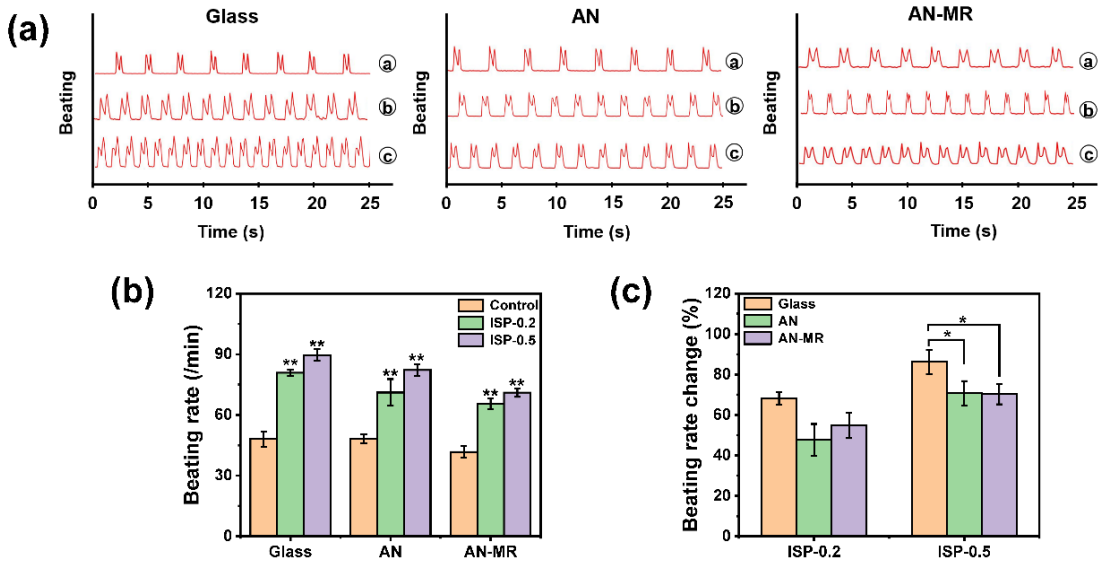

Figure 6. Drug response of the hiPSC-CMs cultured on different substrates to ISP. (a) Representative beating velocity recordings of the hiPSC-CMs on glass, AN and AN-MR substrates in response to ISP with different concentrations (ⓐ: 0; ⓑ: 0.2 μM; ⓒ: 0.5 μM). (b) Beating rate of the hiPSC-CMs on three substrates in response to ISP with different concentrations; *$p < 0.05$ and **$p < 0.01$ compared with control group. (c) Beating rate change percentage of the hiPSC-CMs on three substrates in response to ISP with different concentrations; *$p < 0.05$ compared with glass group.

Inversely, E-4031 as a human ether-a-go-go related gene (hERG) channel blocker can extend Q-T interval and reduce the heart beating rate [16]. An obvious decrease was observed at 50 nM and 100 nM E-4031 in terms of beating frequency and velocity for hiPSC-CMs on all

of the three substrates (Fig. 7(a) and 7(b)). After calculation, the beating rate of hiPSC-CMs decreased by 32.33% and 45.55% on glass, 33.78% and 40.6% on AN group, 33.29% and 35.59% on AN-MR group at 50 nM and 100 nM conditions, respectively (Fig. 7(c)). The results showed that there was no significant difference in beating rate change among the three substrates under the treatment of 50 nM E-4031. As the concentration of E-4031 was further increased, the drug effectiveness in the glass group showed higher variability compared with those observed in AN group and was significantly stronger than that in AN-MR group ($P < 0.05$), which was similar to the findings of Herron et al. [63]. In addition, we also observed the loss of the relaxation peak in doublet contraction/relaxation peaks with the increase of E-4031 concentration, which reflects a slowing relxation by the treatment of E-4031 and it was also consistent with the previous reports [64, 65] .

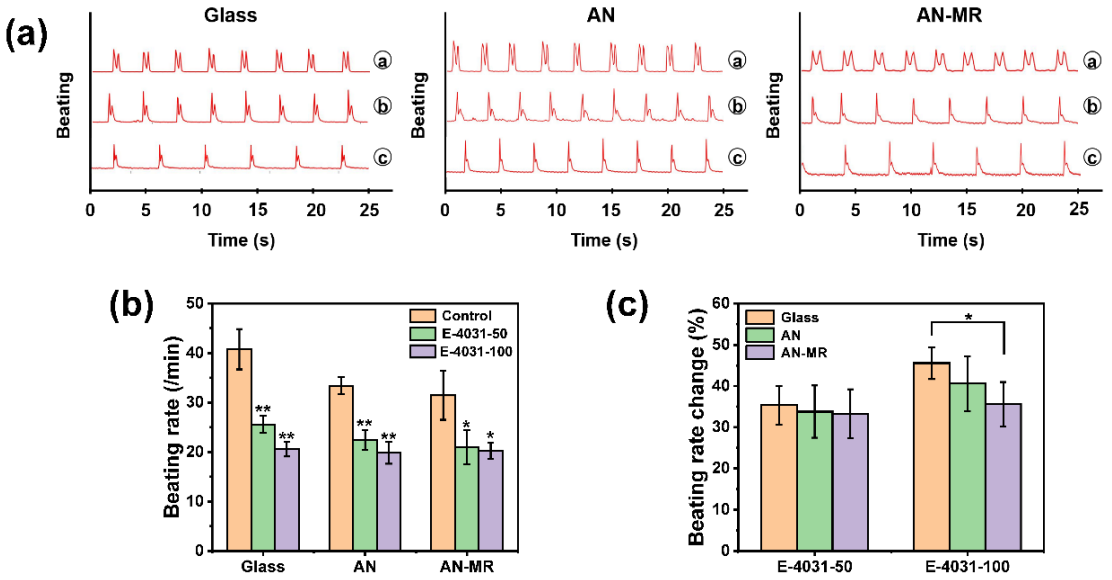

Figure 7. Drug response of the hiPSC-CMs on different substrates to E-4031. (a) Representative beating velocity recordings of the hiPSC-CMs on glass, AN and AN-MR substrates in response to E-4031 with different concentrations (ⓐ: 0; ⓑ: 50 nM; ⓒ: 100 nM). (b) Beating rate of the hiPSC-CMs on three substrates in response to E-4031 with different concentrations; *$p < 0.05$ and **$p < 0.01$ compared with control group. (c) Beating rate change percentage of the hiPSC-CMs on three substrates in response to E-4031 with different concentrations; *$p < 0.05$ compared with glass group.

The above testing results exhibited that the hiPSC-CMs grown on glass substrate exhibited a more evident contractile response to the drug treatment compared with that in AN and AN-MR groups for both E-4031 and ISP. Furthermore, compared with the hiPSC-CMs on AN

substrate, those in AN-MR group were more insensitive to the drugs. It has been reported that the more mature hiPSC-CMs were, the more resistant to drugs they were[61, 66]. It is possible that the weaker drug response of the hiPSC-CMs on AN-MR substrate was in connection with the better functional maturity of the cells. This might be the result that both the off-ground culture environment and the topographic cues provided by the aligned nanofibers of AN-MR substrate synergistically promoted the maturation of hiPSC-CMs. And our findings were also similar to the E-4031 results of Li et al. [67] and ISP results of Wheelwright et al. [68]. The more mature state of hiPSC-CMs can better reproduce the structural and functional properties of *in vivo* adult cardiac cells, which would be more reliable to be applied for *in vitro* drug testing.

The effect of the proposed AN-MR substrate on the structural maturation of hiPSC-CMs has been demonstrated in this work, however, the influence on the function of hiPSC-CMs has not yet been fully understood and demonstrated. It still needs to be further studied by calcium transient and electrophysiological analysis, e.g., field pacing based analysis of inotropy and individual beating waveform changes in response to drug treatment, which will be studied in our future work.

4. Conclusion

In this study, we fabricated a simple micro/nano hierarchical substrate based on soft lithography and electrospinning technology for the *in vitro* endothelium formation and maturation of hiPSC-CMs. Firstly, the cell alignment, proliferation and the endothelial barrier formation of HUVECs on AN-MR substrate were studied and the results showed that AN-MR substrate could promote the alignment of HUVECs and enhanced the integrity of barrier compared with the other control groups. Then, a more adult‐like structural phenotype was achieved in hiPSC‐CMs on AN-MR substrates in terms of myofibril alignment and length, cell length-width ratio and the expression of maturation related genes. In addition to the morphology and structure of hiPSC‐CMs, the final drug testing results proved the more insensitive responses of the hiPSC-CMs on AN-MR substrate to the two typical cardiac drugs, especially as the drug concentration increased. The drug testing results further demonstrated the better functional maturity of the hiPSC-CMs on AN-MR substrate than that in the other groups. Therefore, the topographical cues provided by the aligned nanofibers and the suspended culture environment

supported by the microridges of the proposed AN-MR substrate could achieve a synergistic effect on both the growth and barrier formation of endothelial cells and the maturation of hiPSC-CMs.

Previously, the advantages of aligned nanofibers for endothelium formation and hiPSC-CMs maturation have been widely demonstrated [19, 69, 70]. This work was more focused on the synergistic effect of aligned nanofibrous topography and off-ground culture environment on both endothelium formation and hiPSC-CMs maturation. In the proposed AN-MR substrate, aligned nanofibrous net can provide cells with aligned topographical guidance, while microridges can raise the nanofiber layer up. Combined with the optimized high through-hole percentage of the nanofibrous net, an off-ground culture environment can be formed for cells similar to our previous reports [27, 29, 30]. This kind of off-ground culture could improve cell metabolism because of the increased bottom surface exposure to medium, compared with the other conventional culture ways with only upper surface contact to medium. The findings in this work including the enhanced proliferation and tighter cell-cell junctions of HUVECs, as well as the structural maturation of hiPSC-CMs on AN-MR substrate could be attributed to not only the regulatory effect of the aligned nanofibers on cellular anisotropy, but also the improvement of the off-ground culture environment on cell-medium exchange.

In our future work, the detachment of the formed endothelium layer from AN-MR substrate would be achieved by cell sheet technology and the further application of the endothelial layer could also be studied. The effect of AN-MR substrate on hiPSC-CMs maturation would also be further explored to deeply understand the mechanism of the promotion effect, such as signal pathway modulation and the mechanical interaction between CMs and the substrate.

Notes

The authors declare no competing financial interest.

Acknowledgement

This work was supported by Guangdong Basic and Applied Basic Research Foundation (No. 2023A1515030270), Science and Technology Planning Project of Guangdong Province

(Nos. 2022A0505050074, 2022A0505030014), Science and Technology Program of Guangzhou (No. 202102020645). We would like to thank Analysis and Test Center of Guangdong University of technology for confocal imaging.

References

1. Li, Y.; Huang, G.; Zhang, X.; Wang, L.; Du, Y.; Lu, T. J.; Xu, F., Engineering cell alignment in vitro. *Biotechnology Advances* **2014,** *32* (2), 347-365.

2. Zhang, F.; Qu, K.; Li, X.; Liu, C.; Ortiz, L. S.; Wu, K.; Wang, X.; Huang, N., Gelatin-based hydrogels combined with electrical stimulation to modulate neonatal rat cardiomyocyte beating and promote maturation. *Bio-Design and Manufacturing* **2021,** *4* (1), 100-110.

3. Bliley, J.; Tashman, J.; Stang, M.; Coffin, B.; Shiwarski, D.; Lee, A.; Hinton, T.; Feinberg, A., FRESH 3D bioprinting a contractile heart tube using human stem cell-derived cardiomyocytes. *Biofabrication* **2022,** *14* (2), 024106.

4. Muangsanit, P.; Roberton, V.; Costa, E.; Phillips, J. B., Engineered aligned endothelial cell structures in tethered collagen hydrogels promote peripheral nerve regeneration. *Acta Biomaterialia* **2021,** *126*, 224-237.

5. Choi, J. S.; Lee, S. J.; Christ, G. J.; Atala, A.; Yoo, J. J., The influence of electrospun aligned poly(epsilon-caprolactone)/collagen nanofiber meshes on the formation of self-aligned skeletal muscle myotubes. *Biomaterials* **2008,** *29* (19), 2899-2906.

6. Altomare, L.; Gadegaard, N.; Visai, L.; Tanzi, M. C.; Farè, S., Biodegradable microgrooved polymeric surfaces obtained by photolithography for skeletal muscle cell orientation and myotube development. *Acta Biomaterialia* **2010,** *6* (6), 1948-1957.

7. Chen, S.; Nakamoto, T.; Kawazoe, N.; Chen, G., Engineering multi-layered skeletal muscle tissue by using 3D microgrooved collagen scaffolds. *Biomaterials* **2015,** *73*, 23-31.

8. Kim, W.; Kim, M.; Kim, G. H., 3D-Printed Biomimetic Scaffold Simulating Microfibril Muscle Structure. *Advanced Functional Materials* **2018,** *28* (26), 1800405.

9. Mohindra, P.; Desai, T. A., Micro- and nanoscale biophysical cues for cardiovascular disease therapy. *Nanomedicine: Nanotechnology, Biology and Medicine* **2021,** *34*, 102365.

10. Li, X.; Wang, X.; Yao, D.; Jiang, J.; Guo, X.; Gao, Y.; Li, Q.; Shen, C., Effects of aligned and random fibers with different diameter on cell behaviors. *Colloids and Surfaces B: Biointerfaces* **2018,** *171*, 461-467.

11. Park, D.; Kim, D.; Park, S. J.; Choi, J. H.; Seo, Y.; Kim, D.-H.; Lee, S.-H.; Hyun, J. K.; Yoo, J.; Jung, Y.; Kim, S. H., Micropattern-based nerve guidance conduit with hundreds of microchannels and stem cell recruitment for nerve regeneration. *npj Regenerative Medicine* **2022,** *7* (1), 62.

12. Charbonier, F. W.; Zamani, M.; Huang, N. F., Endothelial Cell Mechanotransduction in the Dynamic Vascular Environment. *Advanced Biosystems* **2019,** *3* (2), 1800252.

13. Shin, Y. M.; Shin, H. J.; Heo, Y.; Jun, I.; Chung, Y.-W.; Kim, K.; Lim, Y. M.; Jeon, H.; Shin, H., Engineering an aligned endothelial monolayer on a topologically modified nanofibrous platform with a micropatterned structure produced by femtosecond laser ablation. *Journal of Materials Chemistry B* **2017,** *5* (2), 318-328.

14. Kim, D.; Eom, S.; Park, S. M.; Hong, H.; Kim, D. S., A collagen gel-coated, aligned nanofiber membrane for enhanced endothelial barrier function. *Scientific Reports* **2019,** *9* (1), 14915.

15. Morimoto, Y.; Nagata, S.; Matsumoto, M.; Sugahara, K.; Miura, S.; Takeuchi, S., Microfluidic system for applying shear flow to endothelial cells on culture insert with collagen vitrigel membrane. *Sensors and Actuators B: Chemical* **2021,** *348*, 130675.
16. Tang, Y.; Tian, F.; Miao, X.; Wu, D.; Wang, Y.; Wang, H.; You, K.; Li, Q.; Zhao, S.; Wang, W., Heart-on-a-chip using human iPSC-derived cardiomyocytes with an integrated vascular endothelial layer based on a culture patch as a potential platform for drug evaluation. *Biofabrication* **2023,** *15* (1), 015010.
17. Tan, S. H.; Ye, L., Maturation of Pluripotent Stem Cell-Derived Cardiomyocytes: a Critical Step for Drug Development and Cell Therapy. *Journal of Cardiovascular Translational Research* **2018,** *11* (5), 375-392.
18. Jiang, Y.; Park, P.; Hong, S. M.; Ban, K., Maturation of Cardiomyocytes Derived from Human Pluripotent Stem Cells: Current Strategies and Limitations. *Molecules and cells* **2018,** *41* (7), 613-621.
19. Takada, T.; Sasaki, D.; Matsuura, K.; Miura, K.; Sakamoto, S.; Goto, H.; Ohya, T.; Iida, T.; Homma, J.; Shimizu, T.; Hagiwara, N., Aligned human induced pluripotent stem cell-derived cardiac tissue improves contractile properties through promoting unidirectional and synchronous cardiomyocyte contraction. *Biomaterials* **2022,** *281*, 121351.
20. Song, M.; Jang, Y.; Kim, S.-J.; Park, Y., Cyclic Stretching Induces Maturation of Human-Induced Pluripotent Stem Cell-Derived Cardiomyocytes through Nuclear-Mechanotransduction. *Tissue Engineering and Regenerative Medicine* **2022,** *19* (4), 781-792.
21. Kumar, N.; Sridharan, D.; Palaniappan, A.; Dougherty, J. A.; Czirok, A.; Isai, D. G.; Mergaye, M.; Angelos, M. G.; Powell, H. M.; Khan, M., Scalable Biomimetic Coaxial Aligned Nanofiber Cardiac Patch: A Potential Model for "Clinical Trials in a Dish". **2020,** *8*.
22. Huethorst, E.; Hortigon, M.; Zamora-Rodriguez, V.; Reynolds, P. M.; Burton, F.; Smith, G.; Gadegaard, N., Enhanced Human-Induced Pluripotent Stem Cell Derived Cardiomyocyte Maturation Using a Dual Microgradient Substrate. *ACS Biomaterials Science & Engineering* **2016,** *2* (12), 2231-2239.
23. Wang, P.-Y.; Yu, H.-T.; Tsai, W.-B., Modulation of alignment and differentiation of skeletal myoblasts by submicron ridges/grooves surface structure. *Biotechnology and Bioengineering* **2010,** *106* (2), 285-294.
24. Zhang, Y.; Zhang, Z.; Wang, Y.; Su, Y.; Chen, M., 3D myotube guidance on hierarchically organized anisotropic and conductive fibers for skeletal muscle tissue engineering. *Materials Science and Engineering: C* **2020,** *116*, 111070.
25. Yeo, M.; Kim, G., Nano/microscale topographically designed alginate/PCL scaffolds for inducing myoblast alignment and myogenic differentiation. *Carbohydrate Polymers* **2019,** *223*, 115041.
26. Yang, L.; Ge, L.; Zhou, Q.; Mokabber, T.; Pei, Y.; Bron, R.; van Rijn, P., Biomimetic Multiscale Hierarchical Topography Enhances Osteogenic Differentiation of Human Mesenchymal Stem Cells. *Advanced Materials Interfaces* **2020,** *7* (14), 2000385.
27. Tang, Y.; Liu, L.; Li, J.; Yu, L.; Wang, L.; Shi, J.; Chen, Y., Induction and differentiation of human induced pluripotent stem cells into functional cardiomyocytes on a compartmented monolayer of gelatin nanofibers. *Nanoscale* **2016,** *8* (30), 14530-14540.
28. Tang, Y.; Liu, L.; Li, J.; Yu, L.; Severino, F. P. U.; Wang, L.; Shi, J.; Tu, X.; Torre, V.; Chen, Y., Effective motor neuron differentiation of hiPSCs on a patch made of crosslinked monolayer gelatin nanofibers. *Journal of Materials Chemistry B* **2016,** *4* (19), 3305-3312.
29. Tang, Y.; Ulloa Severino, F. P.; Iseppon, F.; Torre, V.; Chen, Y., Patch method for culture of primary hippocampal neurons. *Microelectronic Engineering* **2017,** *175*, 61-66.

30. Wang, Y.; Duan, Y.; Tian, F.; Zhou, Z.; Liu, Y.; Wang, W.; Gao, B.; Tang, Y., Ultrathin and handleable nanofibrous net as a novel biomimetic basement membrane material for endothelial barrier formation. *Colloids and Surfaces B: Biointerfaces* **2022,** *219*, 112775.
31. Li, D.; Xia, Y., Electrospinning of Nanofibers: Reinventing the Wheel? *Advanced Materials* **2004,** *16* (14), 1151-1170.
32. Lian, X.; Zhang, J.; Azarin, S. M.; Zhu, K.; Hazeltine, L. B.; Bao, X.; Hsiao, C.; Kamp, T. J.; Palecek, S. P., Directed cardiomyocyte differentiation from human pluripotent stem cells by modulating Wnt/β-catenin signaling under fully defined conditions. *Nature Protocols* **2013,** *8* (1), 162-175.
33. Sharma, A.; Li, G.; Rajarajan, K.; Hamaguchi, R.; Burridge, P. W.; Wu, S. M., Derivation of highly purified cardiomyocytes from human induced pluripotent stem cells using small molecule-modulated differentiation and subsequent glucose starvation. *J Vis Exp* **2015,** (97), 52628.
34. Cortella, L. R. X.; Cestari, I. A.; Lahuerta, R. D.; Araña, M. C.; Soldera, M.; Rank, A.; Lasagni, A. F.; Cestari, I. N., Conditioning of hiPSC-derived cardiomyocytes using surface topography obtained with high throughput technology. *Biomedical Materials* **2021,** *16* (6), 065007.
35. Marsano, A.; Conficconi, C.; Lemme, M.; Occhetta, P.; Gaudiello, E.; Votta, E.; Cerino, G.; Redaelli, A.; Rasponi, M., Beating heart on a chip: a novel microfluidic platform to generate functional 3D cardiac microtissues. *Lab on a Chip* **2016,** *16* (3), 599-610.
36. Xu, C.; Wang, L.; Yu, Y.; Yin, F.; Zhang, X.; Jiang, L.; Qin, J., Bioinspired onion epithelium-like structure promotes the maturation of cardiomyocytes derived from human pluripotent stem cells. *Biomaterials Science* **2017,** *5* (9), 1810-1819.
37. Xiang, L.; Cui, W., Biomedical application of photo-crosslinked gelatin hydrogels. *Journal of Leather Science and Engineering* **2021,** *3* (1), 3.
38. Zhang, D.; Wu, S.; Feng, J.; Duan, Y.; Xing, D.; Gao, C., Micropatterned biodegradable polyesters clicked with CQAASIKVAV promote cell alignment, directional migration, and neurite outgrowth. *Acta Biomaterialia* **2018,** *74*, 143-155.
39. Zhang, D.; Li, Z.; Shi, H.; Yao, Y.; Du, W.; Lu, P.; Liang, K.; Hong, L.; Gao, C., Micropatterns and peptide gradient on the inner surface of a guidance conduit synergistically promotes nerve regeneration in vivo. *Bioactive Materials* **2022,** *9*, 134-146.
40. Han, J.; Wu, Q.; Xia, Y.; Wagner, M. B.; Xu, C., Cell alignment induced by anisotropic electrospun fibrous scaffolds alone has limited effect on cardiomyocyte maturation. *Stem Cell Research* **2016,** *16* (3), 740-750.
41. Nemeno-Guanzon, J. G.; Lee, S.; Berg, J. R.; Jo, Y. H.; Yeo, J. E.; Nam, B. M.; Koh, Y.-G.; Lee, J. I., Trends in Tissue Engineering for Blood Vessels. *Journal of Biomedicine and Biotechnology* **2012,** *2012*, 956345.
42. Yeo, M.; Kim, G., Micro/nano-hierarchical scaffold fabricated using a cell electrospinning/3D printing process for co-culturing myoblasts and HUVECs to induce myoblast alignment and differentiation. *Acta Biomaterialia* **2020,** *107*, 102-114.
43. Ghajarieh, A.; Habibi, S.; Talebian, A., Biomedical Applications of Nanofibers. *Russian Journal of Applied Chemistry* **2021,** *94* (7), 847-872.
44. Dejana, E.; Giampietro, C., Vascular endothelial-cadherin and vascular stability. *Current Opinion in Hematology* **2012,** *19* (3).
45. Huynh, J.; Nishimura, N.; Rana, K.; Peloquin, J. M.; Califano, J. P.; Montague, C. R.; King, M. R.; Schaffer, C. B.; Reinhart-King, C. A., Age-Related Intimal Stiffening Enhances Endothelial Permeability and Leukocyte Transmigration. *Science Translational Medicine* **2011,** *3* (112), 112ra122-

112ra122.
46. VanderBurgh, J. A.; Hotchkiss, H.; Potharazu, A.; Taufalele, P. V.; Reinhart-King, C. A., Substrate stiffness heterogeneities disrupt endothelial barrier integrity in a micropillar model of heterogeneous vascular stiffening. *Integrative Biology* **2018,** *10* (12), 734-746.
47. Lampi, M. C.; Faber, C. J.; Huynh, J.; Bordeleau, F.; Zanotelli, M. R.; Reinhart-King, C. A. J. P. O., Simvastatin ameliorates matrix stiffness-mediated endothelial monolayer disruption. **2016,** *11* (1), e0147033.
48. Kohn, Julie C.; Zhou, Dennis W.; Bordeleau, F.; Zhou, Allen L.; Mason, Brooke N.; Mitchell, Michael J.; King, Michael R.; Reinhart-King, Cynthia A., Cooperative Effects of Matrix Stiffness and Fluid Shear Stress on Endothelial Cell Behavior. *Biophysical Journal* **2015,** *108* (3), 471-478.
49. Di Baldassarre, A.; Cimetta, E.; Bollini, S.; Gaggi, G.; Ghinassi, B., Human-Induced Pluripotent Stem Cell Technology and Cardiomyocyte Generation: Progress and Clinical Applications. *Cells* **2018,** *7* (6).
50. Suh, T. C.; Amanah, A. Y.; Gluck, J. M., Electrospun Scaffolds and Induced Pluripotent Stem Cell-Derived Cardiomyocytes for Cardiac Tissue Engineering Applications. *Bioengineering (Basel)* **2020,** *7* (3).
51. Kartha, C. C., Structure and Function of Cardiomyocyte. In *Cardiomyocytes in Health and Disease*, Kartha, C. C., Ed. Springer International Publishing: Cham, 2021; pp 3-12.
52. Ge, F.; Wang, Z.; Xi, J. J., Engineered Maturation Approaches of Human Pluripotent Stem Cell-Derived Ventricular Cardiomyocytes. *Cells* **2019,** *9* (1).
53. Watson, S. A.; Duff, J.; Bardi, I.; Zabielska, M.; Atanur, S. S.; Jabbour, R. J.; Simon, A.; Tomas, A.; Smolenski, R. T.; Harding, S. E.; Perbellini, F.; Terracciano, C. M., Biomimetic electromechanical stimulation to maintain adult myocardial slices in vitro. *Nature Communications* **2019,** *10* (1), 2168.
54. Carson, D.; Hnilova, M.; Yang, X.; Nemeth, C. L.; Tsui, J. H.; Smith, A. S. T.; Jiao, A.; Regnier, M.; Murry, C. E.; Tamerler, C.; Kim, D.-H., Nanotopography-Induced Structural Anisotropy and Sarcomere Development in Human Cardiomyocytes Derived from Induced Pluripotent Stem Cells. *ACS Applied Materials & Interfaces* **2016,** *8* (34), 21923-21932.
55. Correia, C.; Koshkin, A.; Duarte, P.; Hu, D.; Teixeira, A.; Domian, I.; Serra, M.; Alves, P. M., Distinct carbon sources affect structural and functional maturation of cardiomyocytes derived from human pluripotent stem cells. *Scientific Reports* **2017,** *7* (1), 8590.
56. Kit-Anan, W.; Mazo, M. M.; Wang, B. X.; Leonardo, V.; Pence, I. J.; Gopal, S.; Gelmi, A.; Nagelkerke, A.; Becce, M.; Chiappini, C.; Harding, S. E.; Terracciano, C. M.; Stevens, M. M., Multiplexing physical stimulation on single human induced pluripotent stem cell-derived cardiomyocytes for phenotype modulation. *Biofabrication* **2021,** *13* (2), 025004.
57. Ribeiro, A. J. S.; Ang, Y.-S.; Fu, J.-D.; Rivas, R. N.; Mohamed, T. M. A.; Higgs, G. C.; Srivastava, D.; Pruitt, B. L., Contractility of single cardiomyocytes differentiated from pluripotent stem cells depends on physiological shape and substrate stiffness. *Proceedings of the National Academy of Sciences* **2015,** *112* (41), 12705-12710.
58. Cui, C.; Wang, J.; Qian, D.; Huang, J.; Lin, J.; Kingshott, P.; Wang, P.-Y.; Chen, M., Binary Colloidal Crystals Drive Spheroid Formation and Accelerate Maturation of Human-Induced Pluripotent Stem Cell-Derived Cardiomyocytes. *ACS Applied Materials & Interfaces* **2019,** *11* (4), 3679-3689.
59. Zhang, M.; Xu, Y.; Chen, Y.; Yan, Q.; Li, X.; Ding, L.; Wei, T.; Zeng, D., Three-Dimensional Poly-(ε-Caprolactone) Nanofibrous Scaffolds Promote the Maturation of Human Pluripotent Stem Cells-Induced Cardiomyocytes. *Front Cell Dev Biol* **2022,** *10*, 875278.

60. Andrysiak, K.; Stępniewski, J.; Dulak, J., Human-induced pluripotent stem cell-derived cardiomyocytes, 3D cardiac structures, and heart-on-a-chip as tools for drug research. *Pflügers Archiv - European Journal of Physiology* **2021,** *473* (7), 1061-1085.
61. da Rocha, A. M.; Campbell, K.; Mironov, S.; Jiang, J.; Mundada, L.; Guerrero-Serna, G.; Jalife, J.; Herron, T. J., hiPSC-CM Monolayer Maturation State Determines Drug Responsiveness in High Throughput Pro-Arrhythmia Screen. *Scientific Reports* **2017,** *7* (1), 13834.
62. Jesus, I. C. G.; Araújo, F. M.; Mesquita, T.; Júnior, N. N. S.; Silva, M. M.; Morgan, H. J. N.; Silva, K. S. C.; Silva, C. L. A.; Birbrair, A.; Amaral, F. A.; Navegantes, L. C.; Salgado, H. C.; Szawka, R. E.; Poletini, M. O.; Guatimosim, S., Molecular basis of Period 1 regulation by adrenergic signaling in the heart. *The FASEB Journal* **2021,** *35* (10), e21886.
63. Herron, T. J.; Rocha, A. M. D.; Campbell, K. F.; Ponce-Balbuena, D.; Willis, B. C.; Guerrero-Serna, G.; Liu, Q.; Klos, M.; Musa, H.; Zarzoso, M.; Bizy, A.; Furness, J.; Anumonwo, J.; Mironov, S.; Jalife, J., Extracellular Matrix–Mediated Maturation of Human Pluripotent Stem Cell–Derived Cardiac Monolayer Structure and Electrophysiological Function. *Circulation: Arrhythmia and Electrophysiology* **2016,** *9* (4), e003638.
64. Tadano, K.; Miyagawa, S.; Takeda, M.; Tsukamoto, Y.; Kazusa, K.; Takamatsu, K.; Akashi, M.; Sawa, Y., Cardiotoxicity assessment using 3D vascularized cardiac tissue consisting of human iPSC-derived cardiomyocytes and fibroblasts. *Molecular Therapy - Methods & Clinical Development* **2021,** *22*, 338-349.
65. Nayler, W. G.; Poole-Wilson, P., Calcium antagonists: definition and mode of action. *Basic Research in Cardiology* **1981,** *76* (1), 1-15.
66. Lu, H. F.; Leong, M. F.; Lim, T. C.; Chua, Y. P.; Lim, J. K.; Du, C.; Wan, A. C. J. B., Engineering a functional three-dimensional human cardiac tissue model for drug toxicity screening. **2017,** *9* (2), 025011.
67. Li, J.; Minami, I.; Shiozaki, M.; Yu, L.; Yajima, S.; Miyagawa, S.; Shiba, Y.; Morone, N.; Fukushima, S.; Yoshioka, M.; Li, S.; Qiao, J.; Li, X.; Wang, L.; Kotera, H.; Nakatsuji, N.; Sawa, Y.; Chen, Y.; Liu, L., Human Pluripotent Stem Cell-Derived Cardiac Tissue-like Constructs for Repairing the Infarcted Myocardium. *Stem Cell Reports* **2017,** *9* (5), 1546-1559.
68. Wheelwright, M.; Mikkila, J.; Bedada, F. B.; Mandegar, M. A.; Thompson, B. R.; Metzger, J. M., Advancing physiological maturation in human induced pluripotent stem cell-derived cardiac muscle by gene editing an inducible adult troponin isoform switch. *Stem cells (Dayton, Ohio)* **2020,** *38* (10), 1254-1266.
69. Kim, D.; Eom, S.; Park, S. M.; Hong, H.; Kim, D. S. J. S. r., A collagen gel-coated, aligned nanofiber membrane for enhanced endothelial barrier function. **2019,** *9* (1), 1-11.
70. Chen, Y.; Chan, J. P. Y.; Wu, J.; Li, R.-K.; Santerre, J. P., Compatibility and function of human induced pluripotent stem cell derived cardiomyocytes on an electrospun nanofibrous scaffold, generated from an ionomeric polyurethane composite. *Journal of Biomedical Materials Research Part A* **2022,** *110* (12), 1932-1943.